1.C Satellite Absorption Lines and the Temperature Dependence of X-Ray Absorption Features in High-Temperature Plasmas

In absorption spectroscopy, absorption features impressed on the spectrum of a continuum background source are interpreted in terms of conditions in an absorbing foreground medium. If the opacity per ion for a particular transition beginning from some initial state is known, then the areal density (i.e., the path integral of the density along the path of the continuum propagation) of ions in that state within the absorbing medium can be inferred from the attenuation of the background continuum due to that transition.[1,2] If the relative abundance of ion species can be determined in this way, then temperature can also be inferred from the observed state of ionization, which can be modeled in terms of temperature and density.[2]

In spectra from inertial confinement fusion experiments, the absorption features of interest are unresolved bands of lines from certain ion species, rather than individual lines. The ground configuration and certain low-lying excited configurations of a given ion species each contribute an array of absorption lines to the absorption band of that species. The purpose of this article is to consider the contribution of the excited configurations to the total average absorption strengths of these bands. These excited configurations have not been mentioned explicitly in the earliest published reports on absorption spectroscopy in implosion experiments.[1,2] Among these, the exemplary quantitative analysis by Hauer *et al.*[2] of absorption arrays from an imploded target does not include them. The importance of excited configurations was first considered at the time of this early work,[3] and later by direct comparison of a more complete model[4] with Hauer *et al.*[2] States in the excited configurations have been included in recent detailed models,[4–7] but a general description of the effects of the excited configurations on absorption spectra has yet to be provided. This article aims to provide such a description for two reasons: (1) interesting aspects of these effects can be understood in general terms, and (2) the added insight puts important earlier work into proper perspective.

Ions in the low-lying excited configurations are abundant, and their populations vary widely over the range of temperature found to be typical of conditions in compressed targets. In fact, most of the absorption seen in absorption bands can be due to satellite transitions originating from states in excited configurations. As a result, the total absorption strength per ion of a given species, within a given band, due to all configurations, is temperature dependent and cannot be treated as a constant, as if it were effectively an intrinsic atomic property. Quantitative interpretations of absorption spectra must take this into account.[3]

Laser-driven inertial confinement experiments, particularly the kind where absorption spectroscopy can be used,[1,2] have been described thoroughly elsewhere.[8] In general, they use a small, hollow, spherical target, a

few hundred to several hundred microns in diameter, which is uniformly illuminated with intense laser beams at a total power level of the order of a terawatt for a length of time of the order of a nanosecond. The target, a shell composed mainly of glass, plastic, or both, is either filled with gas or evacuated. Energy absorbed from the laser illumination vaporizes the exterior of the target, which ablates away at high velocity so that the remainder of the target implodes under the force of the reaction to the acceleration of the ablated plasma. Eventually, the imploding shell is stopped by the pressure of the enclosed gas or by the impact when the interior surface of the target meets itself at the center of the implosion. This compression at the center of the target creates conditions of high density and temperature that produce a burst of continuum radiation at or near the time of peak compression. To reach the spectrograph, this radiation passes through what is left of the imploded shell of the target. This unablated remnant of the original target shell is heated during the implosion by compression and a combination of thermal conduction and radiative transport of energy from the outer region of the target that is directly heated by the laser irradiation. The shell remnant can be expected to reach the very broad temperature range where light elements in the neighborhood of chlorine (e.g., silicon through calcium) would be ionized to fluorine-like through helium-like states, the L-shell species.[2] This temperature can vary a great deal, depending on the nature of the experiment, and is typically of the order of a few hundred electron volts, which is an order of magnitude less than the temperatures in the ablation region and in the compressed core. Since these ions have partially vacant L shells, absorption can occur via inner-shell transitions of the kind 1s–2p, which imprints absorption lines on the passing background continuum. These absorbing elements either occur naturally in the shell material itself, e.g., silicon in glass,[1] or they can be introduced as an additive or deposited as a thin concentric layer inside the shell.[2]

At typical shell temperatures, 2s–2p transitions are readily excited by electron collisions, and the excited configurations are heavily populated. The statistical weights of some excited configurations are much larger than those of the respective ground configurations, which can make them even more abundant than the ground configurations, under some conditions. The average 1s–2p absorption strengths of excited configurations are lower than those of ground configurations because the prior 2s–2p excitation has reduced the vacancy of the 2p subshell. The change in 2p vacancy is the primary factor affecting differences in the average 1s–2p absorption strengths among the low-lying configurations of a given species.[3] This reduction is compounded when both 2s electrons are excited, which also occurs readily. Excited oxygen-like and fluorine-like configurations that have full 2p subshells have no 1s–2p opacity at all.

The full spread in excitation energy from the ground state through the excited configurations is roughly 100 eV for the L-shell species of chlorine, which is comparable to, if not less than, the expected shell temperatures. Consequently, the relative populations of the configurations of a given species are temperature dependent. This makes the total 1s–2p absorption

strength per ion, averaged over the same L-shell configurations, temperature dependent as well. Within this range of energy, the states within each configuration are grouped closely in energy. For the relevant species of chlorine, they are typically within 20 eV of each other, often much closer. Since this spread in energy is much less than the anticipated temperatures, the populations of the states within each configuration can be treated, with reasonably good accuracy, as if their populations are distributed relative to each other according to their respective statistical weights. In this approximation, the average 1s–2p opacity per ion within each configuration is independent of temperature.

The terminology "unresolved transition array" has been introduced by Bauche *et al.*[9] to describe the array of lines due to the total of all transitions from one given configuration to another. Statistically weighted configuration averages of line strengths and level populations are the basis for their analysis of broad, unresolved features in x-ray spectra of complex ions. The arrays of lines forming the 1s–2p absorption bands are illustrated in Fig. 45.15 for a few different ionization species of chlorine. The arrays due to each

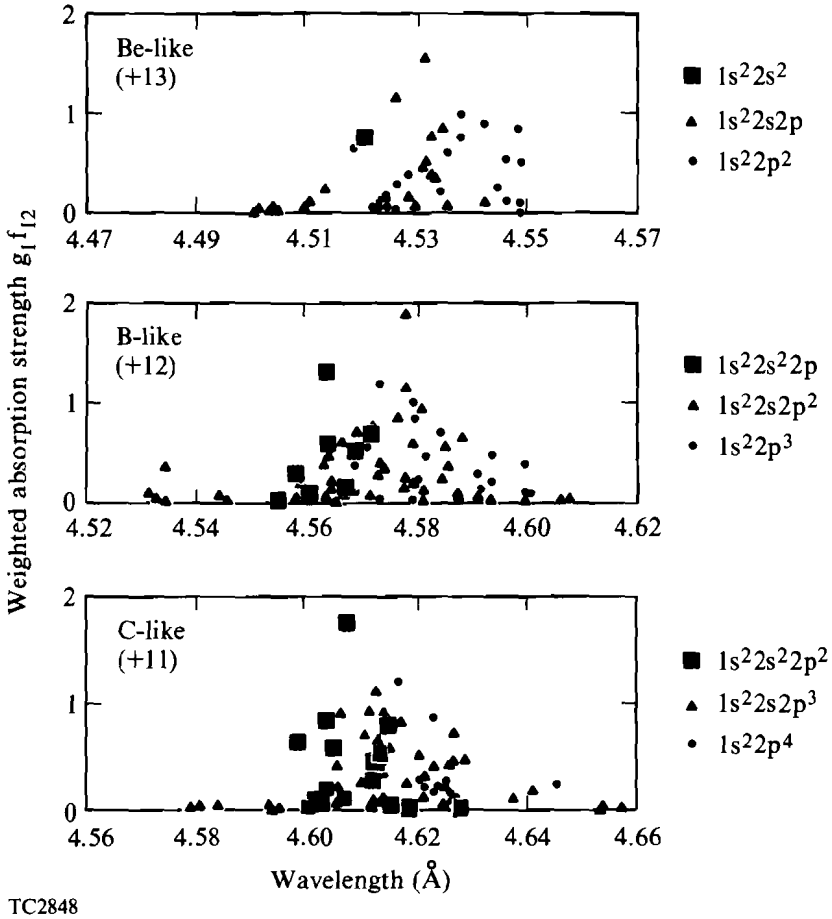

Fig. 45.15
Total statistical-weighted oscillator strengths for all significant (i.e., $g_1 f_{12} > 0.01$) transitions are plotted separately for the beryllium-like, boron-like, and carbon-like ionization species of chlorine. Transitions from the different initial configurations are distinguished. The line arrays from individual configurations are wider than the differences among the average transition energies for each configuration, but the total absorption bands for each species are separate enough to be distinct.

contributing configuration overlap within each band, even though the ranges of energy levels of the different initial configurations do not. Values of the statistically weighted absorption-oscillator strengths $g_1 f_{12}$ for all significant (i.e., $g_1 f_{12} > 0.01$) transitions are plotted at their respective energy. Transitions originating from states in different initial configurations are distinguished by different point symbols. The line arrays for these species are roughly 20 eV in width, which is greater than the differences between the average transition energies for each configuration. The absorption bands for each species are located at energy intervals comparable to their intrinsic width. The shift and broadening of the absorption bands due to temperature-dependent effects on the populations of the initial configurations will be at most only of the order of a few electron volts. Usually, the contribution of excited configuration lines increases the intrinsic widths of the absorption bands only slightly. In the case of the Be-like array, however, the ground configuration has only one allowed 1s–2p transition,[2] so it is specifically the excited configurations that give the total absorption feature the broad appearance of an array of many lines. These results, as well as all other atomic-code results used in this article, were obtained using the relativistic, parameterized potential, multiconfiguration atomic-structure code of Klapisch *et al.*[10]

For the purpose of interpreting an absorption spectrum, it is sufficient to treat each absorption band as a single feature with an effective absorption strength obtained by averaging over all initial configurations, including the excited configurations. The effect of adding the excited configurations to a model of these effective absorption strengths can be expressed as a temperature-dependent correction factor that multiplies the average opacity of the ground configuration. It will be seen that the reduced 2p vacancy of the excited configurations reduces the average opacity of the 1s–2p transitions by as much as about 25% in the high-temperature limit, so estimated areal densities, being inversely proportional to the assumed average opacity, can be low by as much as about 33% if the effect of excited states is not taken into account.

The Correction Factor

The different initial configurations of the absorption transitions of chlorine are separated by 2s–2p transition energies less than about 100 eV, and the energies of the fine-structure transitions within each configuration are much less. With temperatures of the order of 100 eV and with electron densities near 10^{22} cm^{-3} and above, transitions among these L-shell excited states are almost entirely collisional, so their population ratios are fixed by detailed balance between collisional excitation and its inverse. Consequently, the populations P_1 and P_2 of any two such states obey the Boltzmann ratio

$$\frac{P_2}{P_1} = \frac{g_2}{g_1} e^{-(E_2 - E_1)/kT} , \tag{1}$$

where the statistical weights of the two states are g_1 and g_2, respectively, and the respective energies E_1 and E_2 are to be given in the same units as the

temperature kT. At temperatures comparable to the excitation energies, the exponential factor in Eq. (1) is close to unity, and the excited states with large statistical weights can easily be more abundant than the ground state.

The absorption cross section of an individual line is of the form

$$\sigma_i(\nu) = \sigma_i \phi_i(\nu) , \tag{2}$$

where $\phi_i(\nu)$ is the line profile, normalized to unity with respect to frequency ν, and where σ_i is the integrated cross section of the transition. The attenuated intensity $I(\nu)$ remaining after the incident background continuum intensity I_0 passes through a homogeneous layer of thickness Δr of material with a number density N_I of an absorbing species is

$$ln\left(\frac{I_0}{I(\nu)}\right) = N_I \Delta r \frac{\sum_i P_i \sigma_i \phi_i(\nu)}{\sum_i P_i} , \tag{3}$$

where the sum is over all states of the absorbers. The areal density of the absorbing species $N_I \Delta r$ can be obtained from the integrated attenuation and from the total average integrated cross section σ_{tot} using

$$\int ln\left(\frac{I_0}{I(\nu)}\right) d\nu = N_I \Delta r \sigma_{tot} , \tag{4a}$$

where

$$\sigma_{tot} = \frac{\sum_i P_i \sigma_i}{\sum_i P_i} . \tag{4b}$$

A more detailed analysis, including radiation transport with detailed descriptions of line profiles, is needed when the attenuation is complete enough to be unmeasurable,[4,6,11] or when Stark broadening becomes significant enough to have diagnostic value.[7] Otherwise the line profiles need not be considered further.[2]

Equation (4b) is evaluated using P_i from Eq. (1). As was discussed in the introduction, one can assume that the states of each initial configuration occur sufficiently close in energy to the average energy of the configuration for this evaluation to be simplified, following the approach of Bauche *et al.*,[9] by grouping terms in the sum by configuration so that each group represents a single transition array, the statistically weighted sum of all transitions from one configuration to another. In this approximation, the same temperature-dependent exponential applies to all states in each configuration, which leaves these populations fixed relative to each other according to their statistical weights. Equation (4b) then becomes

$$\sigma_{\text{tot}} = \frac{\sum_j g_j \sigma_j e^{-(E_j - E_1)/kT}}{\sum_j g_j e^{-(E_j - E_1)/kT}}, \tag{5}$$

where the index j denotes the initial configurations, $1s^2 2s^2 2p^n$ (ground, $j = 1$), $1s^2 2s 2p^{n+1}$, and $1s^2 2p^{n+2}$, or however many of these have no more than five 2p electrons. E_j and σ_j are now configuration averages and g_j is the total statistical weight of configuration j.

Equation (5) has only one distinct temperature-dependent exponential term for each initial configuration, rather than one term per state, as in Eq. (4b), but these terms do adequately represent the temperature dependence associated with the characteristic excitation energies of each configuration. The effect of this approximation is that all state populations within a configuration change simultaneously as the temperature is varied, rather than in the order of their excitation energy. Since this ordering occurs over small energy differences, compared with anticipated temperatures, errors will also be small, except in the limit where the temperature falls below the energy intervals separating the levels of the ground configuration so that statistical weights alone no longer describe the partition of the ground-configuration populations.

The correct temperature-dependent average cross section can be recovered from the average absorption cross section σ_1 of the ground configuration by applying the correction factor

$$\frac{\sigma_{\text{tot}}}{\sigma_1} = \frac{\sum_j g_j (\sigma_j / \sigma_i) e^{-(E_j - E_1)/kT}}{\sum_j g_j e^{-(E_j - E_1)/kT}}. \tag{6}$$

The differences among the cross sections of the possible initial configurations are primarily due to differences in the vacancy of the 2p subshell. The 2s–2p excitation does change the distribution of spectator charge in the ion, but, to a very close approximation, the ratio σ_j/σ_1 in Eq. (6) can be replaced by the ratio of the 2p vacancies of the two configurations.

The statistical weights, vacancies, and excitation energies needed to evaluate Eq. (6) for the case of chlorine are given in Table 45.II. The excitation energies are the statistical-weight average energy of all states within the indicated configuration, as obtained using the atomic structure code by Klapisch *et al.*[10] The correction factor given by Eq. (6) is shown plotted in Fig. 45.16 as a function of temperature for all the relevant ionization species of chlorine. The total 1s–2p absorption cross section for a particular ionization species is obtained from the total cross section of the ground configuration alone by applying this correction factor. At lower temperatures, the excited configurations are nearly empty, and there is no

Table 45.II: Average parameters for the configurations of chlorine ions.

Configuration	Excitation Energy (eV)	1s–2p Energy (eV)	(Å)	gf	Statistical Weight	2p Vacancy
Helium-like						
$1s^2$		2778.0	4.463	0.882	1	6
Lithium-like						
$1s^22s$		2756.0	4.499	1.559	2	6
$1s^22p$	32.3	2753.0	4.504	3.860	6	5
Beryllium-like						
$1s^22s^2$		2737.0	4.530	0.745	1	6
$1s^22s2p$	32.6	2731.0	4.540	7.594	12	5
$1s^22p^2$	42.6	2728.0	4.545	7.484	15	4
Boron-like						
$1s^22s^22p$		2711.0	4.574	3.657	6	5
$1s^22s2p^2$	39.8	2708.0	4.579	14.705	30	4
$1s^22p^3$	52.3	2705.0	4.584	7.262	20	3
Carbon-like						
$1s^22s^22p^2$		2689.0	4.611	7.090	15	4
$1s^22s2p^3$	49.2	2686.0	4.616	14.230	40	3
$1s^22p^4$	61.4	2683.0	4.621	3.500	15	2
Nitrogen-like						
$1s^22s^22p^3$		2669.0	4.646	6.867	20	3
$1s^22s2p^4$	57.8	2666.0	4.651	6.867	30	2
$1s^22p^5$	69.7	2663.0	4.656	0.676	6	1
Oxygen-like						
$1s^22s^22p^4$		2650.0	4.679	3.288	15	2
$1s^22s2p^5$	65.7	2647.0	4.684	1.317	12	1
$1s^22p^6$	77.3			0.0	1	0
Fluorine-like						
$1s^22s^22p^5$		2632.0	4.711	0.635	6	1
$1s^22s2p^6$	92.4			0.0	2	0

TC2910

correction. At higher temperatures, it is interesting that all the species, except helium-like and lithium-like, approach the same limit of 0.75.

The Screened Hydrogenic Approximation

In evaluating the correction factor from Eq. (6), the same statistical weights and vacancies apply for the L-shell species of other elements; only

the excitation energies differ. To obtain these excitation energies, average configuration energies from the screened hydrogenic approximation[12–15] are convenient. From comparisons with results from numerical atomic-structure calculations shown below, it can be seen that the screened hydrogenic approximation is adequate.

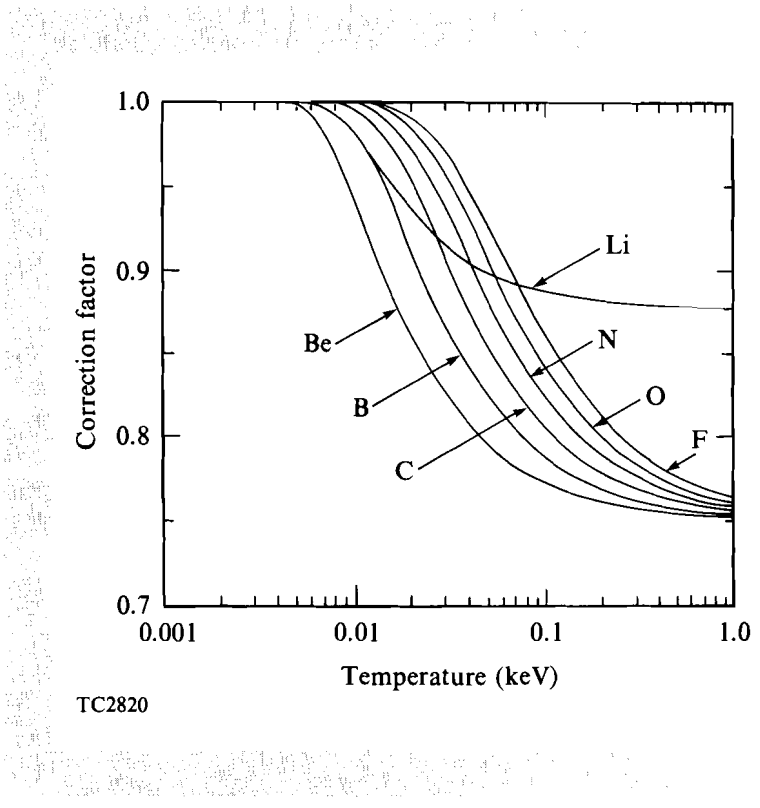

Fig. 45.16
The correction factor given by Eq. (6) is plotted for the relevant ionization species of chlorine. The total 1s–2p absorption cross section for a particular species is obtained from the total cross section of the ground configuration alone by applying the appropriate factor.

In the screened hydrogenic approximation, the energy of any one bound electron is calculated as if it were a single electron bound by a point nucleus whose effective charge is that of the bare nucleus Z minus the effective screening contribution due to the other electrons.[12] The screening of the nuclear charge, as it is seen by an electron in a particular shell, is given by the number of electrons in each shell multiplied by the appropriate respective screening coefficient for each shell.[13] This approach is very convenient for applications where errors of several percent in level energies are not serious.[14,15] These coefficient sets are usually given in terms of the occupation numbers of the principal quantum shells only. Slater's original screening coefficients distinguish between certain subshells, but the s and p subshells are treated as one shell.[12] Mayer has derived two tables of screening coefficients, one in terms of principal quantum shells only, and a shorter table, up to $n = 3$, where the different subshells are distinguished.[13] These are shown in Tables 45.III(a) and 45.III(b), respectively.

The total energy of an ion, in rydbergs, is obtained from the energies E_n and occupation numbers p_n of each principal shell n using the expression

$$E_{\text{ion}}(Ry) = \sum_n p_n E_n \ . \tag{7a}$$

The energy of each shell is given by the hydrogenic expression

$$E_n = -\left(\frac{Q_n}{n}\right)^2 , \tag{7b}$$

where Q_n is the effective nuclear charge seen by the electrons in shell n, where n is the principal quantum number of that level.[13] Level n can be either a shell or a subshell. The effective charge, according to the prescription of Mayer, is given by

$$Q_n = Z - \sum_{m \neq n} p_m \sigma_{nm} - p_n \left(1 - \frac{1}{g_n}\right) \sigma_{nn} , \tag{8}$$

where g_n is the capacity of shell n and the screening coefficients σ_{nm} specify the effect of the electrons in shell m on the screened charge.[13,16] This prescription applies whether the shells are entire principal shells or individual n,l subshells.[13] The prescription of More is nearly the same, except that the values of the screening coefficients are slightly different, and the effective screened charge is given by

$$Q_n = Z - \sum_{m<n} p_m \sigma_{nm} - \frac{1}{2} p_n \sigma_{nn} , \tag{9}$$

where the sum is over only the shells interior to the n^{th} shell and only principal shells are considered.[14]

The values of the first set of coefficients by Mayer, shown in part in Table 45.III(a), are very close to the more recent values of More, shown in part in Table 45.IV(a). The latter were obtained by fitting the coefficients to known ionization energies. More does not give coefficients for distinct n,l subshells.[14] For the calculations reported here, the coefficient table of More has been split into subshells in direct proportion to the splitting done in going from the first table of Mayer to the second, Table 45.III(b). This new split set is shown in Table 45.IV(b). Mayer's coefficients and prescription give the needed approximate results, but the split More coefficients, used with a particular modification of Eq. (9), give results that are closer to atomic-structure-code results for the chlorine ions of interest. The modifications in the prescription are that the sum in Eq. (7) is taken over subshells, and that one uses

$$Q_{n,l} = Z - \sum_{m<n} \sum_{l'} p_{m,l'} \sigma_{n,l;m,l'} - \frac{1}{2} \sum_{l'} p_{n,l'} \sigma_{n,l;n,l'} \tag{10}$$

instead of Eq. (9). Here, m and n are principal quantum numbers. The additional sum is taken over all the angular momentum values, $0 \leq l' \leq m-1$, of a shell of principal quantum number m. In Eq. (10), no distinction is made between subshells l' that are interior or exterior to the subshell l.

Table 45.III: Mayer screening coefficients σ_{nm} with and without splitting of the principal subshells.[13]

(a)

$m\backslash n$	1	2
1	0.6250	0.9383
2	0.2346	0.6895

(b)

$m\backslash n$	1s	2s	2p
1s	0.6250	0.8395	0.9712
2s	0.2099	0.6016	0.6494
2p	0.2428	0.6494	0.7266

TC2911

Table 45.IV: Splitting of More screening coefficients σ_{nm}[14] according to the subshell splitting of Mayer.[13]

(a)

$m\backslash n$	1	2
1	0.3125	0.9380
2	0.2345	0.6038

(b)

$m\backslash n$	1s	2s	2p
1s	0.3125	0.8392	0.9709
2s	0.2098	0.5268	0.5678
2p	0.2427	0.5679	0.6363

TC2912

Equation (10) does give improved approximate agreement for L-shell chlorine ions, compared with results obtained with the Mayer prescription, which justifies its use for other elements near chlorine, e.g., from silicon through calcium. Nevertheless, extending More's prescription to separate n,l subshells beyond the neighborhood of L-shell chlorine ions deserves a careful and truly comprehensive treatment, which has not been done here.

Using the energies of L-shell states obtained from the modified More prescription, correction factors for the carbon-like species of silicon, chlorine, and calcium are evaluated from Eq. (6) and plotted in Fig. 45.17. The changes in the correction curves for the other species are very similar. The dotted line is the carbon-like chlorine curve from Fig. 45.16, which was derived using average excitation energies from the atomic-structure code.[10] The close agreement between the two chlorine curves shows that the use of the modified screening prescription is adequate for this purpose. As the nuclear charge changes by about 50%, over the range of elements from silicon ($Z = 14$) through calcium ($Z = 20$), the correction curve shifts in temperature by less than a factor of 2. Other than this displacement in temperature, which reflects the change in the 2s–2p excitation energy, the curves are very similar.

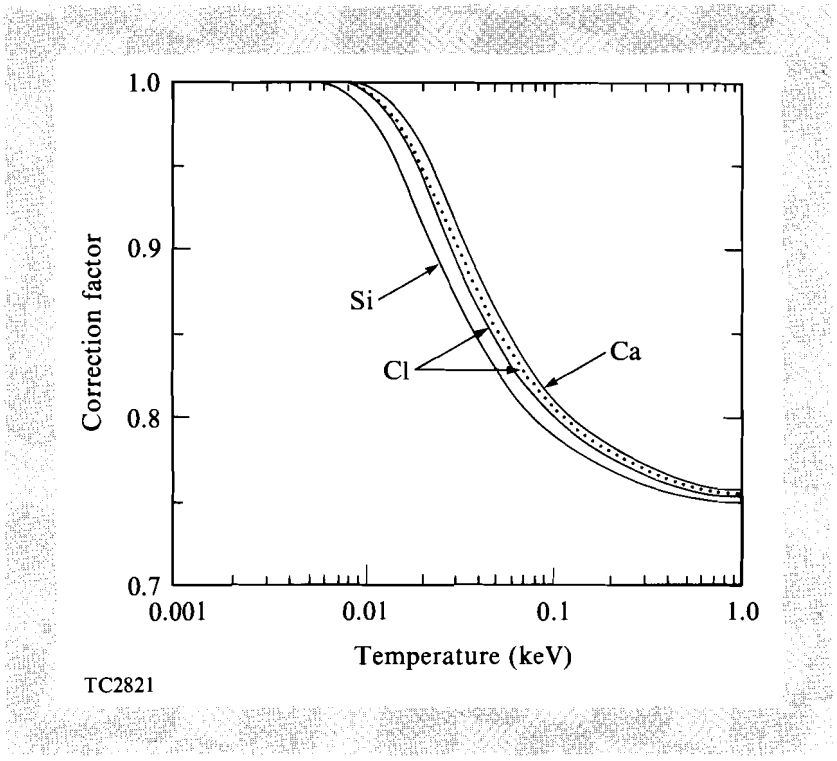

Fig. 45.17
The temperature-dependent absorption correction factor changes relatively little over the range of elements from silicon through calcium, as is shown here for the carbon-like species. Excitation energies used to calculate the solid curves were obtained using the screened hydrogenic approximation. The dotted line is the carbon-like chlorine curve from Fig. 45.16, which was derived from average excitation energies obtained using results from the atomic-structure code.[10]

Scaling of Absorption Strengths

To illustrate the distribution and relative strengths of the 1s–2p transitions of the L-shell ionization species, Fig. 45.18 shows an artificial chlorine spectrum where the lines represent the contribution of each initial configuration to the average oscillator strength of all the 1s–2p transitions of each ionization species. The averaging over each species is done with respect to the statistical weight of the initial state of each individual transition. The species are helium-like through fluorine-like, and the three possible initial configurations are $1s^2 2s^2 2p^n$ (ground), $1s^2 2s 2p^{n+1}$ (singly excited), and $1s^2 2p^{n+2}$ (doubly excited), subject to the restriction that there be no more than six 2p electrons in the final state. Lines are positioned at the average transition energy for the initial configuration they represent. The mean array energies from the initial configurations of a given species are closely spaced, as is also apparent in Fig. 45.15. These results have been obtained from detailed numerical atomic-structure calculations.

The crosses in Fig. 45.18 are configuration-averaged absorption strengths that have been scaled from the helium-like absorption strength in Table 45.II, assuming that they scale with the square of the transition energy and with the vacancy fraction of the initial 2p subshell. The relative strengths of the configuration averages within each species agree extremely well, and the agreement in general is reasonably good. A small adjustment in the assumed transition-energy scaling would compensate for most of the discrepancy. Even though the spectator charge in these ions varies from 1e to 8e (nearly half the nuclear charge, in the case of chlorine), this scaling is seen to account for nearly all the variation in the average absorption strength from configu-

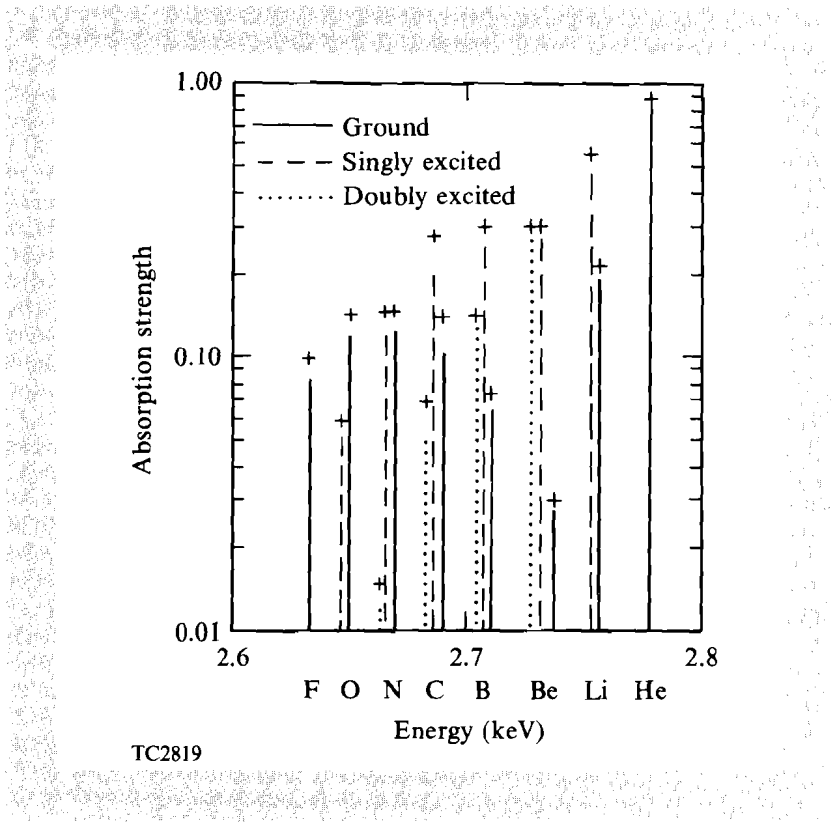

Fig. 45.18
This artificial spectrum is a plot of the average 1s–2p absorption strengths of the possible initial configurations of the helium-like through fluorine-like ionization species of chlorine. Lines are positioned at the average transition energies. The crosses are values scaled from the helium-like absorption strength given in Table 45.II. Scaling with the square of the transition energy and with the vacancy fraction of the initial 2p subshell is seen to account for nearly all of the changes in the average absorption strength.

ration to configuration and from species to species. In particular, the absorption strengths for each initial configuration in any species do indeed occur in very close proportion to their respective 2p vacancy fractions, consistent with the assumption used in evaluating Eq. (6). This scaling is illustrated for the specific case of chlorine, but it can be expected to apply comparably well to the L-shell species of other elements in the neighborhood of chlorine.

Conclusions and Summary

In calculating the line opacity of shell material for the purpose of absorption spectroscopy, most of the absorption can be due to states in excited, and even doubly excited configurations. The temperature-dependent thermal partition of ions into excited configurations results in the temperature dependence of the strengths of the absorption bands. The effect of the excited configurations on the average absorption strength of each species can lead to areal densities underestimated by as much as 33%, if they are not taken into account. Even though other effects, such as inhomogeneities in temperature and density and the nonuniform sampling of the shell by a compact continuum source, can introduce comparable uncertainties and ambiguities into estimates of areal densities, the effect of the excited configurations is systematic and should not be neglected.

This article describes in general terms the effects of these excited configurations, not only as a point of scientific interest, but as a means of

putting into proper perspective the important earlier work that omits these configurations.[2] Since the effects of these excited configurations have been shown to be modest, this article serves to validate this earlier work to within reasonable limits.

ACKNOWLEDGMENT

This work was supported by the U.S. Department of Energy Division of Inertial Fusion under agreement No. DE-FC03-85DP40200 and by the Laser Fusion Feasibility Project at the Laboratory for Laser Energetics, which has the following sponsors: Empire State Electric Energy Research Corporation, New York State Energy Research and Development Authority, Ontario Hydro, and the University of Rochester.

REFERENCES

1. B. Yaakobi, R. L. McCrory, S. Skupsky, J. A. Delettrez, P. Bourke, H. Deckman, C. F. Hooper, and J. M. Soures, *Opt. Commun.* **34**, 213 (1980); A. Hauer, in *Spectral Line Shapes*, edited by B. Wende (W. de Gruyter & Co., Berlin, 1981); D. K. Bradley, J. D. Hares, and J. D. Kilkenny, Rutherford-Appleton Laboratory, Annual Report No. RL-83-043, 1983, p. 5.4.
2. A. Hauer, R. D. Cowan, B. Yaakobi, O. Barnouin, and R. Epstein, *Phys. Rev. A* **34**, 411 (1986).
3. LLE Review **24**, 169 (1985).
4. C. Fievet, Thèse de Doctorat, Paris XI University, Orsay, France, 1989.
5. S. J. Davidson *et al.*, *Appl. Phys. Lett.* **52**, 847 (1988).
6. C. Chenais-Popovics *et al.*, *Phys. Rev. A* **40**, 3194 (1989). Further details of this work are described in Ref. 4.
7. R. C. Mancini and C. F. Hooper, *Rev. Sci. Instrum.* (in press); private communication.
8. R. S. Craxton, R. L. McCrory, and J. M. Soures, *Sci. Am.* **255**, 68 (1986).
9. C. Bauche-Arnoult, J. Bauche, and M. Klapisch, *J. Opt. Soc. Am.* **68**, 1136 (1978).
10. M. Klapisch, *Comp. Phys. Comm.* **2**, 239 (1971); M. Klapisch, J. L. Schwob, B. S. Fraenkel, and J. Oreg, *J. Opt. Soc. Am.* **67**, 148 (1977).
11. J. Balmer *et al.*, *Phys. Rev. A* **40**, 330 (1989).
12. J. C. Slater, *Phys. Rev.* **36**, 57 (1930).
13. H. Mayer, Los Alamos Scientific Laboratory Report AECD-1870 (LADC-464), 1947, decl. 1948.
14. R. M. More, *J. Quant. Spectrosc. Radiat. Transfer* **27**, 345 (1982).
15. R. Marchand, S. Caille, and Y. T. Lee, *J. Quant. Spectrosc. Radiat. Transfer* **43**, 149 (1990).
16. G. C. Pomraning, *The Equations of Radiation Hydrodynamics* (Pergamon, New York, 1973).